AAAI Workshop on Cmputer Vision for Medical Image Processing, San Francisco, CA, March 1994

Reconstructing 3-D Blood Vessel Shapes from Multiple X-Ray Images

Henry A. Rowley and **Takeo Kanade**
har@cs.cmu.edu, tk@cs.cmu.edu
Computer Science Department
Carnegie Mellon University

Introduction

Angiography is a method used by radiologists to examine the structure and health of blood vessels. The method consists of injecting an x-ray opaque contrast agent into the bloodstream, and taking one or more x-ray images of the vessel. Although these images are clear and have high resolution, they individually show structures in only two-dimensions. The goal of our work is to automatically reconstruct the three-dimensional structure of a blood vessel using a small number of angiogram images taken from different angles.

Among the types of information about blood vessels that are useful to physicians, the most important for diagnostic purposes is a measure of the cross-sectional area of the vessel at every location along its length. This information reveals constrictions caused by blood clots, cholesterol build-ups, or injuries. Treatment of these conditions may involve inserting a catheter, with a small video camera and scraping tool mounted at its tip, into the vessel to remove the obstruction. A computer can aid in planning this surgery by simulating what the tip of the catheter would encounter in the vessel, and by computing how far the catheter must be inserted to begin repair.

This paper presents an algorithm which performs the three-dimensional reconstruction task. Each section of the paper will examine one of the main steps of the algorithm: detecting vessels in single images, finding the positions of the vessels in three dimensions, and finally performing diameter measurements. The paper concludes with some reconstruction results.

Finding Vessels in Single Images

The first step in the reconstruction process is to locate vessels in single x-ray images, like the one shown in Figure 1a, or the subtracted image shown in Figure 1b. The subtracted image is produced by subtracting two x-rays, one taken with the contrast agent in the bloodstream, and one without. Subtracted images have enhanced contrast between the vessels and background. As with all images in this paper, black represents low x-ray intensity, and white high intensity, which is the reverse of normal x-ray films. The result of the detection step will be a set of approximate locations of the vessels in one or more images.

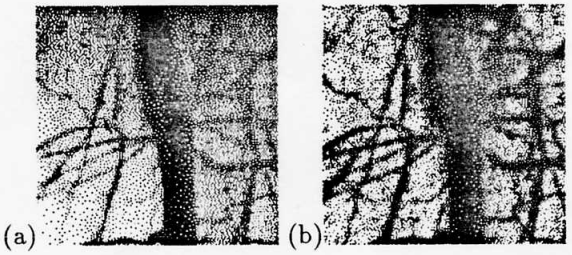

Figure 1: The angiograms shown here will be used to demonstrate the vessel detection algorithm: a) image of an artery in the thigh. b) the result of subtracting an x-ray taken without any contrast agent in the vessel from the image in a. (Courtesy of Dr. Mark Wholey at Shadyside Hospital, Pittsburgh, PA)

A similar problem exists in detecting vessels in images of the retina. [Chaudhuri *et al.*, 1989] applied a collection of linear filters to images of vessels in the retina, each tuned to a specific vessel orientation. For each location in the image, their algorithm records which filter gave the highest response. Using filters tuned to one specific vessel diameter is sufficient in the retinal image domain. However, the variation in vessel size is much larger in the angiogram x-ray domain, which necessitates using multiple filter sizes. When the set of filters is applied at one location in an image, the filter with the maximum response will indicate the size and orientation of a vessel that passes through that location. The filter designs are based on a physical model of the appearance of vessels in an x-ray image.

Physical Model

In order to design a matched filter, we must develop a model of the appearance of a blood vessel in an angiogram x-ray. The model here follows the one in [Kitamuro *et al.*, 1988]. An x-ray beam is diminished fractionally by the materials it passes through. Thus, the logarithm of the beam's intensity will be proportional to the sums of the depths of the materials passed through multiplied by the logarithm of their opacities. If we assume the background is constant, then the darkening of a portion of the image due

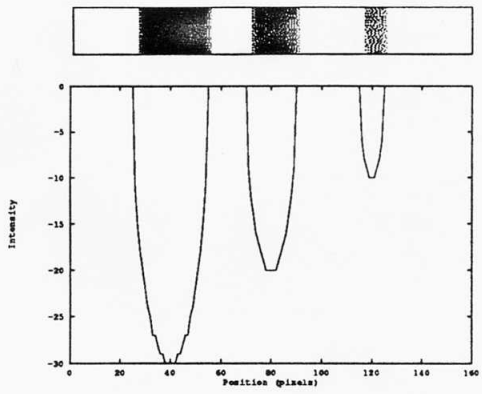

Figure 2: The box shows a synthetic image of vessels with radii of (from left to right) 15, 10, and 5 pixels. The graph shows the intensity along a horizontal line in the image.

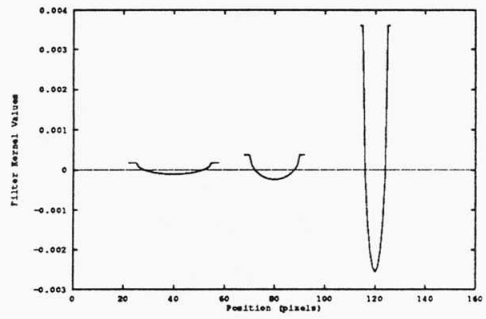

Figure 3: Cross-sections of matched filters tuned to vessels with radii of (from left to right) 15, 10, and 5 pixels.

to a blood vessel will be proportional to the vessel's depth perpendicular to the image plane. If we further assume that the vessel's center line is locally in a plane parallel to the image plane, and has a circular cross-section, then intensity profile across the vessel will have the following form:

$$B + 2\sqrt{r^2 - x^2} \cdot \log O$$

where B is the background intensity, O is the opacity of the vessel (a number between 0 and 1), r is the vessel's radius, and x is the distance between point where the intensity is being computed and the vessel's center line. Figure 2 illustrates this model with a synthetic image of three vessels of different radii, each with the same opacity value, and a background intensity of zero.

Filter Design

As discussed in [Chaudhuri *et al.*, 1989], the optimal filter for detecting an even, real valued signal is the signal itself. Thus matched filters are produced by synthesizing images of a short segment of a vessel of a particular size and orientation. The filter images are normalized to have an average value of zero. When applied to images with a constant or linear background,

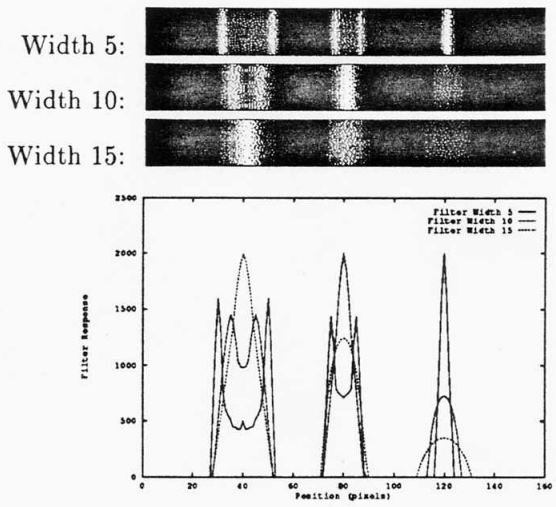

Figure 4: The images show the responses of the three filters applied to the synthetic image in Figure 2, and the graph plots the responses along a horizontal line across the image.

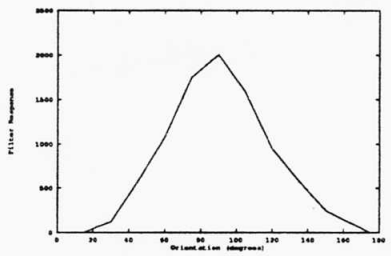

Figure 5: Response of different orientations of the radius 5 filter, when placed over the radius 5 vessel.

or zero mean noise, such normalized filters will give a response of zero. One difficulty is that since the filters for thicker vessels are larger, their responses will have a higher magnitude compared with filters for narrower vessels. This problem was not addressed in [Chaudhuri *et al.*, 1989], as in retinal images, the vessels were all detectable using one filter size. In angiogram images, the difference in size between the largest and smallest vessels is often as high as a factor of twenty, so multiple size filters are needed. To resolve this problem, the filter images are further normalized so that for a constant opacity, each filter will give the same magnitude response when applied to a vessel of the size and orientation to which it is tuned. Cross-sections of filters tuned to vessels in Figure 2 are shown in Figure 3. Figure 4 shows the response of three vertically oriented filters tuned to radii of 5, 10, and 15 pixels are moved across the image in Figure 2. Figure 5 shows the angular sensitivity of the filters, by plotting the response for filters of different orientations when applied over a vessel. In each case, the

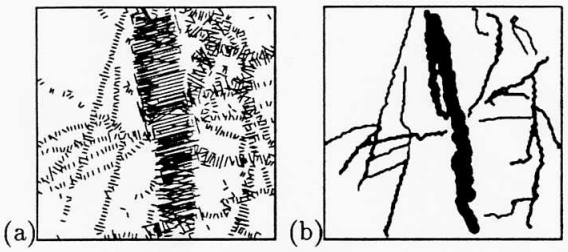

Figure 6: Vessel detection results: a) the angle and size of the filter that responded best at each pixel in the angiogram of Figure 1b, represented by the orientation and length of line segments. b) the result of applying the heuristic edge linking process to the results shown in a. The line thickness is proportional to the average of the sizes of the filters that responded along the edge.

filters give their highest response when applied to the vessel size and orientation to which they are tuned.

Post-Processing

As can be seen in the filter response in Figure 4, as a filter is moved across a corresponding size vessel in the direction perpendicular to the vessel's orientation, the response will reach a local maximum when the filter is over the center of the vessel. Therefore, after a filter is applied to an x-ray image, a ridge detector can more precisely locate the vessels. The ridge detector suppresses all filter responses where the magnitude of the response is not a local maximum in the direction perpendicular to the vessel.

With the filter designs in hand, we can process each x-ray image as follows:

- Compute the logarithm of the intensity of each pixel
- For each filter tuned to a specific size and orientation:
  - Apply the filter to the image
  - Apply a ridge detector to the filter results
- Record the size and orientation of the filter that gave the highest magnitude response for each pixel

One characteristic of the matched filters visible in Figure 4 is that small filters can respond at the edges of a larger vessel, with one side of the filter matching the edge. To solve this problem, we examine each pixel (in order from the largest to the smallest magnitude filter response), assume that it represents the center of a vessel, and suppress any filter responses that might be due to the vessel's edges. Finally, we use the thresholding method of [Otsu, 1979] to suppress weak filter responses. The results of all these steps applied to the image in Figure 1b are shown in Figure 6a. The figure shows the direction and size of the filter that gives the best response at each pixel location.

Edge Linking

The output from the above filtering process is a collection of pixels which may be part of the center line of a vessel. The next step is to perform edge tracking, to link pixels together into curves which may represent vessels. The edge tracking is performed using a local graph search technique guided by a heuristic function, as described in [Gonazalez and Woods, 1992]. The algorithm maintains a collection of possible edges, and selected edges with higher heuristic ratings for extending with more pixels. The most highly weighted component of the evaluation function measures the maximum "error" along the edge so far. This error indicates, for each position along the edge, the difference between the size and orientation of a pixel compared with the average of the sizes and orientations of the previous few pixels along the edge. In case of ties in the error measure, comparisons are made based on the number of consecutive pixels along the curve at which no filter responded. This allows the edges to jump over small gaps, but penalizes large jumps. Finally, in case of ties in that measure, the total number of jumps over no response pixels is used. The result of running the edge linking algorithm on the above filtering result gives Figure 6b. Many slight changes can be made to these heuristics, resulting in different edges being linked together. However, the precise details are not significant, as only approximate localization of the vessels is needed for the next step of the algorithm.

Locating Vessels in Three Dimensions

Starting with the two-dimensional location results of the previous section, we can use multiple images to localize blood vessels in three dimensions. To find the three-dimensional path of the center line of the vessel, we use the snakes algorithm [Kass *et al.*, 1987]. Snakes are defined as a connected sequence of positions in space, each of which can move about in three dimensions. Each node experiences forces in the plane of an image which pull towards dark areas, to align curve with a vessel, and internal forces which keep the curve from developing sharp corners. By combining forces from several images taken at different angles, the snake is moved into alignment with the three-dimensional position of the vessel's center line.

The results from the vessel detection in single images are not yet integrated with this part of the program. At present we initialize the snake by manually selecting its start and end points, and linearly interpolating between them.

Measuring Vessel Diameters

The final step is to measure the diameters of the vessels. Just as a curve was used to model the center line of the vessel, a flexible cylindrical surface is used to represent the vessel's actual shape [Terzopoulos *et al.*, 1987]. The complete model used to represent a vessel's shape is shown in Figure 7. To measure the diameter of a vessel, the program examines the intensity profile across the vessel, and matches this with an expected intensity profile similar to the one used to design the matched filters [Kitamuro *et al.*, 1988]. This model has six parameters which are varied with

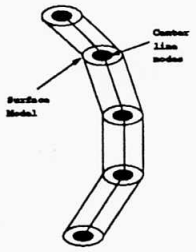

Figure 7: Model used to represent a blood vessel.

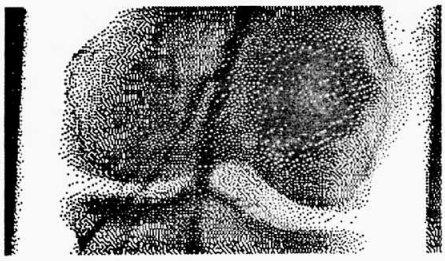

Figure 8: An angiogram image, showing arteries in the knee. (Courtesy of Dr. Mark Wholey at Shadyside Hospital, Pittsburgh, PA)

a non-linear fitting algorithm to find the best fit. The diameter parameter estimate is used to apply forces to the flexible surface model, deforming it into alignment with the vessel's shape.

Results and Conclusions

The system has been tested with three sequences of angiogram images, provided by Shadyside Hospital in Pittsburgh, PA, which show arteries in the pelvis, thigh, and knee. Figure 8 shows one frame from the latter sequence, and Figure 9 presents the three-dimensional reconstruction of the main vessel and one of its branches. Note that a constriction in the main vessel, below the branch, has been successfully reconstructed.

The current program requires a some manual input to set the initial position estimates of the blood vessel center lines. Work is in progress to automate the task of detecting vessels in single images, and to integrate this with the three-dimensional localization process.

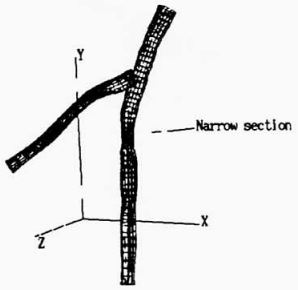

Figure 9: Reconstruction of the vessels shown in Figure 8.

An important consideration in this work is that for the reconstructions to be useful, they must be accurate. While it may not be possible to compare the model with direct physical measurements, it is possible to use other imaging modalities such as Computed Tomography (CT) and ultrasound to cross-check the results. We are arranging with Shadyside Hospital (where the x-rays were obtained) to perform such comparisons.

Acknowledgements

We greatfully acknowledge the contributions of Dr. Mark Wholey and Katherine Hill at Shadyside Hospital, who provided the x-ray image data and other information. Thanks are also due to Shumeet Baluja for his careful reading of drafts of this paper.

This work was supported in part by the Avionics Laboratory, Wright Research and Development Center, Aeronautical Systems Division (AFSC), U.S. Air Force, Wright-Patterson Air Force Base, OH 45433-6543, under Contract F33615-C1465, ARPA Order No. 7597. The views and conclusions contained in this document are those of the authors and should not be interpreted as representing the official policies, either expressed or implied, of ARPA or the U.S. government.

References

[Chaudhuri *et al.*, 1989]
Subhasis Chaudhuri, Shankar Chatterjee, Norman Katz, Mark Nelson, and Michael Goldbaum. Detection of blood vessels in retinal images using two-dimensional matched filters. *IEEE Transactions on Medical Imaging*, 8(3):263–269, September 1989.

[Gonazalez and Woods, 1992] Rafael C. Gonazalez and Richard E. Woods. *Digital Image Processing.* Addison-Wesley Publishing Company, Reading, Massachusetts, 1992.

[Kass *et al.*, 1987] Michael Kass, Andrew Witkin, and Demetri Terzopoulos. Snakes: Active contour models. In *Proceedings of the First International Conference on Computer Vision*, pages 259–268, 1987.

[Kitamuro *et al.*, 1988] Koichi Kitamuro, Jonathan M. Tobis, and Jack Sklansky. Estimating the 3-D skeletons and transverse areas of coronary arteries from biplane angiograms. *IEEE Transactions on Medical Imaging*, 7(3):173–176, 1988.

[Otsu, 1979] Nobuyuki Otsu. A threshold selection method from gray-level histograms. *IEEE Transactions on Systems, Man, and Cybernetics*, SMC-9:62–66, January 1979.

[Terzopoulos *et al.*, 1987] Demetri Terzopoulos, Andrew Witkin, and Michael Kass. Symmetry-seeking models for 3-D object recognition. In *Proceedings of the First International Conference on Computer Vision*, page 269, 1987.

140, Santa Clara, CA, February 12-13, 1990.

[Lazzaro et al., 1988] J. Lazzaro, S. Ryckebusch, M.A. Mahowald and C. Mead, "Winner-Take-All Networks of O(n) Complexity," in *Advances in Neural Information Processing Systems Vol. 1*, D. Tourestzky, ed., pp. 703-711, Morgan Kaufmann, San Mateo, CA, 1988.

[Mahowald and Mead, 1989] M.A. Mahowald and C. Mead, "Silicon Retina," Chap. 15 of *Analog VLSI and Neural Systems*, Addison-Wesley Publishing Co., 1989.

[Mathur and Koch, 1991] B. Mathur and C. Koch, *Visual Information Processing: From Neurons to Chips*, eds., *Proc. SPIE*, Vol. 1473, 1991.

[Mead 1989] C. Mead, *Analog VLSI and Neural Systems*. Reading, MA: Addison-Wesley, 1989.

[Shafer et al., 1994] Shafer, S.A, T. Kanade, and K. Ikeuchi, "Image Understanding at CMU", in these proceedings, 1994.

[Van der Spiegel et al., 1989] J. Van der Spiegel, G. Kreider, C. Claeys, I. Debusschere, G. Sandini, P. Dario, F. Fantini, P. Bellutti and G. Sondini, "A Foveated Retina-Like Sensor Using CCD Technology, "Chap. 8 of *Analog VLSI Implementation of Neural Systems*, C. Mead and M. Ismail, eds., Kluwer Academic Publishers, 1989.

[Standley, 1991] D. Standley, "An Object Position and Orientation IC with Embedded Imager," *IEEE Journal of Solid-State Circuits*, Vol. 26, No. 12, pp. 1853-1860, 1991.

[Veldkamp and McHugh, 1992] W. B. Veldkamp and T. J. McHugh, "Binary Optics," *Scientific American*, May 1992.

[Weckler, 1967] Weckler, G.P. "Operation of p-n Junction Photodetectors in a Photon Flux Integrating Mode," IEEE Jour. of Solid–State Circuits, pp. 65–73, Vol. sc–2, No. 3, September, 1967

[Wyatt et al., 1990] J.L. Wyatt Jr., D. Standley and B. Horn, "Local Computation of Useful Global Quantities Using Linear Resistive-Grid Networks," poster session, *Conf. on Neural Networks for Computing*, Snowbird, UT, April 1990.

[Yu et al., 1992] P.C. Yu, S.J. Decker, H.S. Lee, C.G. Sodini and J.L. Wyatt, Jr., "CMOS Resistive Fuses for Image Smoothing and Segmentation," *IEEE Journal of Solid-State Circuits*, Vol. 27, No. 4, pp. 545-553, April 1992.